ROYAL SOCIETY OF CHEMISTRY

PAPER

Check for updates

A simple microscopy approach quantifies biomineralized CO$_2$ in *Coccolithus braarudii* – a calcifying marine phytoplankton†

Toby Morton-Collings,[a] Minjun Yang, [iD] [a] Christopher Batchelor-McAuley,[a] Samuel Barton,[b] Rosalind E. M. Rickaby,[b] Heather A. Bouman[b] and Richard G. Compton [iD] *[a]

Climate is partly controlled by atmospheric carbon dioxide levels. In turn atmospheric CO$_2$ is substantially regulated by oceanic phytoplankton, specifically coccolithophores which biomineralize CO$_2$ as CaCO$_3$ in the form of tiny platelets which ultimately sink to the ocean floor. The scale of this biomineralization is massive; some 10^{15} g of CaCO$_3$ are formed by phytoplankton per annum. This figure represents a tiny mass of CaCO$_3$ per phytoplankton multiplied by a huge number of individual coccolithophores. For modelling the climate, it is essential to measure the biomineralized CaCO$_3$ at single entity as well as bulk level. In this work we show that a simple light microscopy approach can, by monitoring the undersaturation driven dissolution of calcite in deionised (DI) water, quantify sub-nanograms of calcite mass of heterococcoliths secreted by marine phytoplankton. We show that the biogenic calcite found in coccoliths dissolves at a comparable mass-transport rate to that of inorganic particulate calcite in DI water. We further show that undersaturation driven dissolution is not suitable for quantifying coccolithophores due to competing osmotic pressure effects.

Environmental significance

Calcifying marine phytoplankton, coccolithophores, sequester dissolved CO$_2$ in the form of CaCO$_3$ in the open ocean at a rate that is directly comparable to the rate of CO$_2$ released by humans. Their extent of CO$_2$ sequestration, on both a single entity and bulk level, reflects any changes due to environmental stressors and changes in their local biogeochemistry and thus is an important indicator for climate change. Presently, there is no good way of routinely measuring the mass of biomineralized calcite on a single-entity level. We address this issue by utilising the undersaturation dissolution of biogenic CaCO$_3$ to reveal their calcite mass on a single-entity level.

Introduction

The surface ocean is supersaturated with respect to calcium carbonate (CaCO$_3$).[1] Coccolithophores, the dominant pelagic calcifiers, biomineralize calcium carbonate in the open surface water at an annual gigatonne scale (>10^{15} g per year) and encrust themselves with interlocking plates of calcite, generated intracellularly, called coccoliths.[2,3] This biomineralized particulate inorganic carbon (PIC) plays a crucial role in the marine carbon cycle removing alkalinity from surface waters[4] so that the ocean sequesters atmospheric CO$_2$ by ballasting the export of organic carbon to the deep ocean where carbon can be stored for millennia.[5,6] The amount of CO$_2$ burial depends on the ratio

of inorganic carbon (CaCO$_3$) to organic carbon that sinks to the deep ocean.[7] However, under the uncertainties associated with climate change, laboratory results show species-specific responses to changes in conditions such as CO$_2$ partial pressure, temperature and pH.[8–10] The fate and the extent of coccolithophore calcification, which began ~209 million years ago,[11] may be jeopardised by the rapid changes in the local biogeochemistry associated with the current climate crisis. The sustainability of the marine carbonate cycle and CO$_2$ fixation is presently at risk. Therefore, simple and accessible methodologies measuring the extent of coccolithophore calcification at the single entity level in different laboratory conditions are crucial to understanding the cellular response to various stressors.

Current methods in accurately quantifying the PIC mass of individual coccoliths without knowledge of the species, including for example the coccolith shape factor,[12] are not without limitations and are summarised elsewhere.[13] Briefly, these methods are esoteric involving bespoke microscopy setups combined with either electrogenerated acid to 'titrate'

[a]*Physical and Theoretical Chemistry Laboratory, Department of Chemistry University of Oxford, South Parks Road, Oxford, UK. E-mail: Richard.Compton@chem.ox.ac.uk*

[b]*Department of Earth Sciences, University of Oxford, South Parks Road, Oxford, UK*

† Electronic supplementary information (ESI) available. See DOI: https://doi.org/10.1039/d2va00252c

© 2023 The Author(s). Published by the Royal Society of Chemistry

Environ. Sci.: Adv., 2023, **2**, 645–651 | **645**

away the calcium carbonate[13] or utilising the birefringent optical properties of calcite to infer its thickness.[14–17] While birefringence is limited to individual coccolith PIC quantification, recent advances in the opto-electrochemical acid 'titration' approach allow the $CaCO_3$ content of entire living coccolithophores to be inferred at a cellular level.[18] Sophisticated 3-D reconstruction of coccolithophores is feasible using X-ray tomography but this requires high-energy synchrotron light sources and cannot be accessed for routine measurements.[19]

In this work, we developed a straightforward light microscope method, simple in comparison to alternatives[14–19] as reviewed elsewhere and discussed below,[13] to measure the PIC content of individual heterococcoliths and living coccolithophores, comprising the interlocking coccosphere of coccoliths using a conventional optical microscope. We utilise the sparing solubility of $CaCO_3$ in aqueous solutions (solubility constant of 3.3×10^{-9} M^2 at 298 K)[1] together with the observation of the dissolution of biogenic calcite particles to infer their PIC masses. The work first studies the dissolution of coccoliths in de-ionised (DI) water before the focus turns to living coccospheres.

Experimental section

Chemicals

Deionised Water (MilliQ ultrapure, resistivity 18.2 MΩ cm^{-1} at 298 K) was used to make up all solutions. Sodium chloride and other chemicals were purchased from Scientific Laboratory Supplies, UK, and used without further purification.

Cultures

Cultures of *Coccolithus pelagicus* subsp. *Braarudii* (RCC1198) were supplied by the Roscoff Culture Collection (RCC), France. The cultures were maintained on a K/2 enriched growth medium modified from the recipe for K medium by Keller *et al.* with f/2 vitamins.[20] Aquil synthetic ocean water was used instead of natural seawater.[21] The final molarity of each of the medium components in the K/2 recipe is summarized elsewhere.[13,18] Stock cultures of RCC 1198 underwent regular subculturing into fresh growth medium under sterile conditions during the exponential growth phase. The culture was kept under a 14 : 10 hours light–dark cycle with a light intensity of 20–40 μmol quanta m^{-2} s^{-1} at 17 °C in a PHCbi MLR-352-PE Incubator (PHC Europe B.V.). Note that the two-fold range in light intensity received by the culture medium arises depending on where the sample is positioned relative to the light source within the incubator and the variation in the turbidity of the medium throughout the growth curve.

Optical microscopy

Two optical microscopes were used to observe the coccoliths and coccospheres in this work. The still image of the *C. braarudii* coccolith shown in Fig. 1b was taken using a 40× objective lens (numerical aperture 0.7–1.3, Carl Zeiss, UK) and a Hamamatsu ORCA-flash 4.0 C13440 CMOS camera (Hamamatsu,
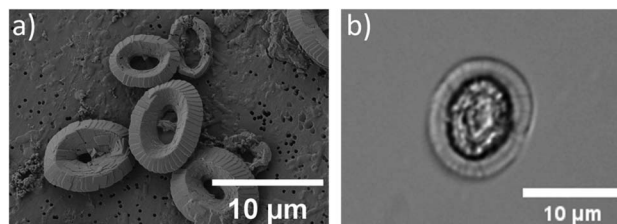

Fig. 1 Images of *C. braarudii* coccoliths obtained *via* (a) scanning electron microscopy and (b) optical microscopy using a 40× objective lens under bright-field illumination.
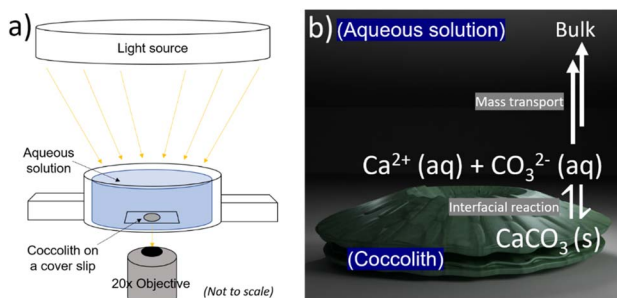

Fig. 2 (a) Schematic of the microscope setup used to monitor the dissolution of coccoliths aqueous solution. The biogenic particle of interest is illuminated by a bright-field and imaged using a 20× objective lens. (b) Schematic of the calcite dissolution reaction at the coccolith–water interface.

Japan) on an upright microscope (Zeiss AXIO Examiner, Carl Zeiss, UK).

The biogenic calcite dissolution experiments were performed on openFrame.[22] The openFrame microscope was supplied by Cairn Research Ltd, UK in 2020. A custom 3D printed 'Petri dish', an illustration of which is shown in Fig. 2a, was used as a supporting substrate for the biogenic $CaCO_3$ samples. The 3D STL file of the custom 'Petri dish' can be found in the ESI Files† and downloaded online. Optical images were recorded using a 20× objective (Numerical Aperture = 0.5, Olympus, Japan) and a Hamamatsu ORCA-flash 4.0 C13440 CMOS camera (Hamamatsu, Japan) providing 16-bit, 4-megapixel images. The bright-field light source was provided by Aura Pro phase contrast illuminator (Cairn Research Ltd, UK). Fig. S7 in the ESI† shows the entire inverted microscope setup involving the openFrame, custom printed 'Petri dish', light source and the camera arrangement.

Scanning electron microscopy

The phytoplankton culture containing the coccoliths was filtered using a polycarbonate filter (0.01 μm), washed with deionized water, and subsequently dried at atmospheric pressure. Prior to the imaging, 10 nm of a gold thin-layer was coated over the sample using a rotary pumped coater (Q150RES, Quorum, UK). The Scanning Electron Microscopy (SEM) images were obtained using a Sigma 300 FEG-SEM from Zeiss with an accelerating voltage of 2.0 kV.

Biogenic calcite dissolution: procedure & analysis

The 3D printed Petri dish was filled with aqueous solutions resulting in a solution depth of at least 1 cm. The *C. braarudii* culture sample, prewashed with $CaCO_3$ saturated aqueous solution, was shaken before a 20 μL aliquot was dropcasted into the Petri dish (see Fig. 2 below). The pre-washing procedure minimises unwanted salt transferred from the culture medium into the aqueous solution. The biogenic calcite: coccoliths and coccospheres, were allowed to sediment onto the coverslip for 10–20 seconds before imaging. During this period, the 'Petri dish' was sealed with parafilm to limit evaporation induced convection over the timescale of the dissolution experiment. Optical acquisition of 10 seconds per frame then began until the biogenic calcite completely dissolved. The setting up took no more than 30–60 s from the immersion of the particles to the start of the recordings. A minor readjustment of optical focus was required during the video acquisition due to the long experimental timescale (1–2 hours). The images recorded were analysed with ImageJ freeware (Fiji distribution) to provide a measure of the particle projection area as a function of time. The 3D coccolith reconstruction method was described in previous work.[13]

Results and discussion

In the following, the dissolution of detached *C. braarudii* coccoliths is first monitored in pure, deionised (DI) water. We aim to answer the following questions: (1) is it possible to infer the mass of individual coccoliths from a simple dissolution experiment? (2) Does biogenic calcite dissolve at the mass-transport limit as that seen with inorganic calcite?[23,24] Then, the focus turns to study the auto-dissolution of living coccosphere in aqueous solutions.

Dissolution of coccoliths in DI water: dissolution kinetics

Fig. 1a and b show representative SEM and optical images of detached *C. braarudii* coccoliths. The dimensions of the coccoliths are of the micron scale with a coccolith length (major axis) measuring around 10 μm. As can be seen in the SEM image, the coccolith size found within a culture is not uniform resulting in a variation in the coccolith PIC mass from one coccolith to another.[13] Therefore, a simple, non-esoteric and cheap approach allowing the PIC contents of individual biogenic calcite particulates to be obtained (coccolith and/or entire coccosphere) is desirable for routine monitoring.

Fig. 2a is a schematic showing the experimental set-up involving a *C. braarudii* coccolith immersed in DI aqueous solution (with no added Ca^{2+}, CO_3^{2-} or other ions). Optical images of the coccolith were recorded under bright-field illumination as a function of time. At the coccolith–solution interface, illustrated in Fig. 2b, the following interfacial reaction takes place until equilibrium is established

$$CaCO_3(s) \rightleftharpoons Ca^{2+}(aq) + CO_3^{2-}(aq) \tag{1}$$
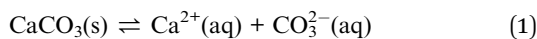
However, since the bulk solution is in overwhelmingly excess (~20 mL) relative to the coccolith and the ions $Ca^{2+}(aq)$ and $CO_3^{2-}(aq)$ are absent, the biogenic calcite will dissolve to completion long before the aqueous solution is saturated with respect to $CaCO_3$. Fig. 3a shows snapshots of a representative *C. braarudii* coccolith undergoing auto-dissolution in DI water. A timelapse video can be found in the online article (coccolith.avi). The top row of Fig. 3a shows raw images of the coccolith as a function of time following the initial immersion and the bottom row shows images after auto-thresholding. Interestingly, at $t \approx 3000$ s the coccolith begins to disintegrate into many small units of calcite 'blocks'[25] which hints that the alternating crystalline unit of the coccolith may be held together by mechanical tension during nucleation and growth as opposed to some form of 'natural glue'. Fig. 3b plots the projection area of the coccolith on the imaging plane as a function of time. Note that with the experimental setup used, the bright LED light source for bright-field illumination increases the temperature of the DI water bath by no more than 4 Kelvin from the initial temperature (293 ± 1 K) over the course of the experiment. The vertical dotted grey line indicates the timepoint at which the coccolith begins to fall apart and the projection area of the coccolith can no longer be accurately measured. A linear decrease of the projection area of the coccolith can be seen before the structural disintegration occurs and has a slope of -0.015 μm^2 s^{-1}. The solid lines overlaid in Fig. 3b are calculated for a hypothetical calcite cuboid when placed on a plate, with dimensions similar to the coccolith, dissolving in DI water at the mass-transport limit.[26] The blue and red lines are calculated for 291 K and 298 K, respectively, using the temperature-sensitive calcite solubility constant and diffusion coefficients.[23] Note that the calculation, detailed in ESI Section 1,† accounts for the calcite density of the coccolith by using the coccolith shape factor reported by Young *et. al.*[12] The shape factor of *C. pelagicus* ranges from 0.04–0.07 and a recommended value of 0.06 was used herein which adds ~±20% uncertainty to the above calculation. As can be seen, within the possible range of temperature fluctuations during the experiment, the accuracy of coccolith projection area measurement, and the approximation of the coccolith shape to that of a cuboid with equivalent dimensions, the experimentally obtained rate of dissolution of *C. braarudii* coccolith is in excellent agreement with that calculated for a similar sized hypothetical calcite cuboid. Therefore, we conclude that the dissolution rate of the coccolith in DI water occurs at the mass-transport limit and is indistinguishable from a cuboid of equivalently sized inorganic calcite. This result is suggestive that any organic or inorganic contaminants of coccolith calcite must be present at such trace levels that they have minimal impact on the calcite solubility, and is fully consistent with the reported reanalysis[23] of the data reported by Hassenkam *et al.* obtained using atomic force microscopy.[24]

Dissolution of coccoliths in DI water: 3D volume reconstruction and PIC mass calculations

In the above, kinetic information of the coccolith auto-dissolution was obtained using a microscope. In this section, we aim to use kinetic data extracted *via* microscopy to infer the
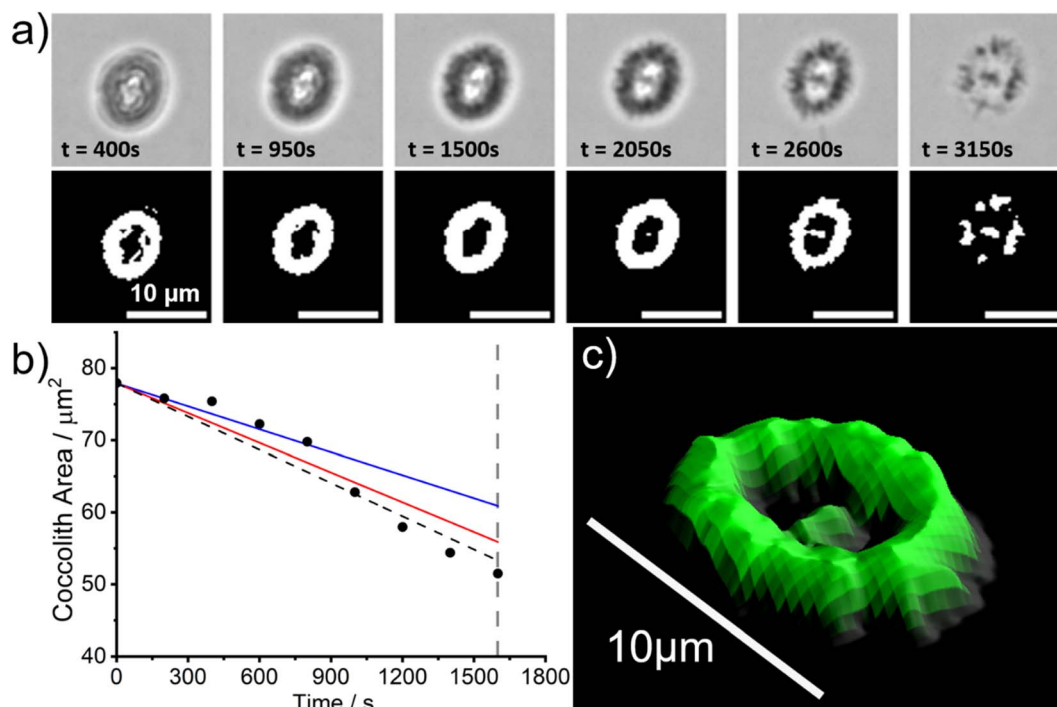
© 2023 The Author(s). Published by the Royal Society of Chemistry

Environ. Sci.: Adv., 2023, **2**, 645–651 | **647**

Fig. 3 (a) Dissolution of a *C. braarudii* (RCC1198) coccolith in DI water at 293 K as a function of time. The top row shows the raw images and the bottom row shows the binary images after auto-thresholding. Scale bar = 10 μm. (b) A plot of the measured coccolith projection area as a function of time. The mass-transport limited rates of dissolution of a cuboid with a similar dimension are shown as solid lines: blue – 291 K and red – 298 K. The dotted black line is a linear line of best fit of the experimental data (black circles) through the initial coccolithophore area measured at $t = 0$ s. The dotted grey line indicates the time at which the projection area of the coccolith can no longer be accurately measured due to the disintegration of the coccolith. (c) 3D reconstructed coccolith from the stack of auto-threshold images, assuming the lateral dissolution rate of the coccolith is equal to the vertical dissolution rate.

PIC mass of coccoliths on a single-entity basis. The analysis involves 3D reconstruction of the coccolith prior to dissolution using the time-stack of 2D optical images (Fig. 2a).[13]

For the 3D coccolith reconstruction, we assume the rate of coccolith dissolution, or rate of shrinkage, as measured on the image plane (X, Y) is the same as that in the orthogonal direction (Z), corresponding to the coccolith height/thickness. First, the lateral coccolith shrinkage in its unilateral direction (m s^{-1}) was obtained by finding the square root of its projection area ($\sqrt{\text{area}} \approx$ length). The change in coccolith length as a function of time is obtained for each individual coccolith. The example shown in Fig. 3b has a shrinkage rate of 1.1 nm s^{-1}. The unilateral rate of shrinkage, measured on a per coccolith basis, is then used in combination with the binary image of the coccolith (bottom row of Fig. 3a up until the time corresponded to complete dissolution). This reveals the heterogeneity of the coccolith in the X–Y direction as provided by the binary images and also the heterogeneity of the coccolith thickness (Z direction) at each of the X and Y coordinates. This allows the coccolith volume prior to the auto-dissolution to be reconstructed.[13] A representative 3D image of the coccolith dissolved in DI water is shown in Fig. 3c, more of which can be found in the ESI in Fig. S2.† The volume of the coccolith shown in Fig. 3c is 92 ± 2 μm^3 which equates to 250 ± 5 pg of calcite after upscaling with the density of calcite ($\rho_{\text{CaCO}_3} = 2.71$ g cm^{-3}).

The black circles in Fig. 4 plot the PIC measurements of 8 individual *C. braarudii* coccoliths found using the 3D reconstruction method. The thickness of the reconstructed coccoliths were in the range of 1–2 μm, which is in excellent agreement with that measured *via* scanning electron microscopy (Fig. S1†). The green shade in Fig. 4 is the estimated coccolith PIC mass using a literature-reported shape factor (f) ranging from 0.04–0.07 for *Coccolithus pelagicus*; where the PIC mass was obtained by PIC mass = $\rho_{\text{CaCO}_3} f l^3$, and l is the coccolith length. The excellent agreement seen validates the coccolith PIC mass obtained *via* 3D reconstruction.

Confirmation of mass-transport control of coccolith auto-dissolution

We have established above that the auto-dissolution of coccolith in DI water occurs at the mass-transport limit. An alternative approach to validate this conclusion to that taken above is to take a hypothetical calcite cuboid with an equivalent dimension to the coccolith and calculated the maximum amount of CaCO$_3$ that can diffuse away in the mass-transport limit over the experimental time seen to fully dissolve the coccolith. The steady-state mass-transport flux (J_{MT}) to a cuboid on a plate has been reported[26]

$$J_{\text{MT}}\left(\text{mol s}^{-1}\right) = \frac{\text{dmoles}}{\text{d}t} = \frac{11.65 D \Delta c L(t)}{4} \quad (2)$$
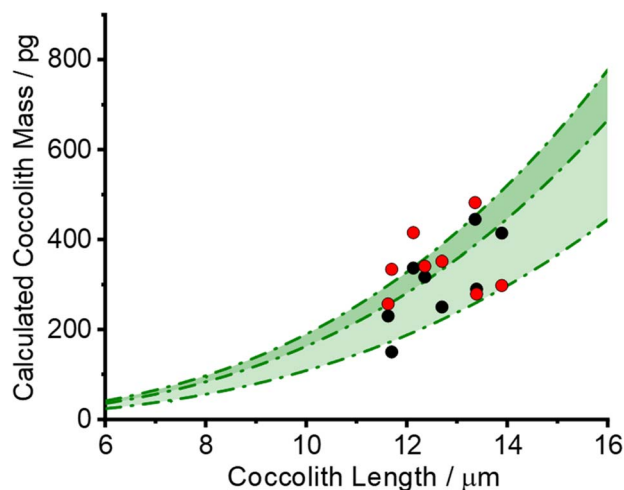
Fig. 4 A plot of coccolith PIC mass against the coccolith length. (Black circles) 3D coccolith reconstruction. (Green lines) PIC mass estimated using the literature reported shape factor, $f = 0.4$, 0.6 and 0.7, for *Coccolithus pelagicus*; PIC mass $= \rho_{CaCO_3} f L^3$. (Red data) PIC mass estimated for calcite cuboids with geometry similar to that of the coccolith under mass-transport control.

where D is the geometric average diffusion coefficient of Ca^{2+} and CO_3^{2-}, Δc is the difference in concentration at the interface and the bulk. The area of the cuboid in contact with the plate is $(L_x L_y)$ equivalent to that of the coccolith $(A_{coccolith} = L_x L_y)$, and the height of the cuboid (L_z) is taken to be 1/10th its side length $(L_{x,y})$, which is approximately the ratio of coccolith thickness to its length (see Fig. S1†). Note that the side-length of the cuboid, generally termed L, appearing in eqn (2) varies as a function of time t reflecting the decrease in the coccolith projection area as it dissolves. By integrating eqn (2) from time following immersion ($t = 0$) to the timepoint when the coccolith was seen to dissolve completely ($t_{dissolve}$), the total moles of $CaCO_3$ that can be dissolved under the mass-transport limit for a hypothetical stubby cuboid with equivalent dimensions of the coccolith are obtained

$$\int_0^{t_{dissolve}} dmoles = \frac{11.65 D \Delta c}{4} \int_0^{t_{dissolve}} L(t) dt \qquad (3)$$

Eqn (3) was solved numerically using the measured projection area of the coccolith. The red circles overlaid in Fig. 4 are the $CaCO_3$ mass calculated for hypothetical equivalent calcite cuboids if they were to dissolve at the mass-transport limited rate under the conditions as the coccoliths studied. Excellent agreement is seen with that obtained *via* 3D coccolith reconstruction (this work) and using the literature reported coccolith shape factor (Young *et al.*).[12] This firmly confirms that the dissolution of coccolith in DI water occurs at the mass-transport limit. Next, we investigate the auto-dissolution of living *C. braarudii* coccolithophores.

Auto-dissolution of *C. braarudii* coccosphere

In the experiments reported in this section, living *C. braarudii* coccolithophores were immersed in aqueous solutions under

similar conditions as the above-studied coccoliths. A SEM image of a *C. braarudii* coccolithophore is shown in Fig. S3.† Fig. 5a shows the images of a living *C. braarudii* coccolithophore undergoing auto-dissolution in DI water. ESI Videos† can be found online in the web version (Coccosphere_DIwater.avi). Fig. 5b plots the projection area of the coccosphere as a function of time after immersion in DI water. Interestingly, initially, the coccosphere was seen to increase in size until *ca.* $t = 4000$ s before particulate "shrapnel" appears from the coccosphere and diffuses outwards resulting in a rapid decrease in the coccosphere size. The increase in size is likely due to an increase in osmotic pressure resulting from the underlying biological cell changing from the artificial sea-water abruptly to a low-ionic strength aqueous solution (DI water). To validate this hypothesis, two coccolithophores were placed in a DI solution saturated with respect to $CaCO_3$. A gradual increase in the coccosphere size, Fig. S4a,† can be seen 2 hours following immersion. After 18 hours of immersion, shown in Fig. S4b,† the projection area of two *C. braarudii* individuals was seen to increase by 33 and 45% which firmly evidences the expansion of coccolithophore size likely due to osmotic pressure. On a more ecologically relevant osmolarity range, small deviations of salinity of seawater have a negligible effect on the coccolithophore cell volume.[27] However, in DI water and in the absence of Ca^{2+} and CO_3^{2-}, unlike the detached coccoliths, the initial dissolution rate of the coccosphere before the appearance of shrapnel is unmeasurable due to the opposing size-changing effects, namely osmotic pressure and auto-dissolution of calcite.

After an immersion time of *ca.* 4000 s in DI water, a rapid decrease in the coccosphere size was seen once fragments of
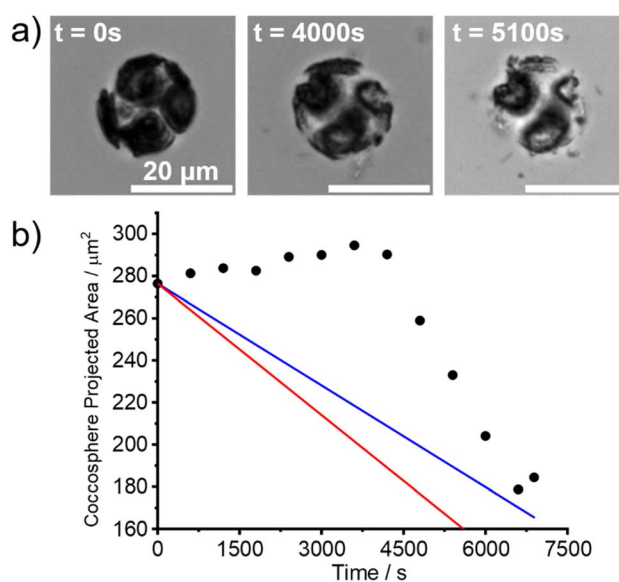

Fig. 5 Dissolution of a living *C. braarudii* coccolithophore in DI water. (a) Microscope images of a coccolithophore at $t = 0$, 4000 and 5100 s. (b) (Black dots) Projection area of the coccosphere measured over time. The blue and red lines are the theoretical changes in the projection area of a hypothetical calcite sphere dissolving in DI water at the mass-transport limit at 291 K and 298 K, respectively.

coccosphere, assumed to be CaCO$_3$, began to appear. The rate of decrease in its projection area occurred at a rate approximately twice as fast compared to the mass-transport limit of an equivalent hypothetical calcite sphere (ESI Section 1†). ESI Section 3† investigates the effect of ionic strength of the aqueous solution on the dissolution of living coccolithophores. As expected, with an increase in the ionic strength of the aqueous solution, the time required to completely dissolve the coccosphere decreased. This is because the solubility constant of calcite increases with ionic strength.[1] A ESI Video† showing the dissolution of a representative coccolithophore in 0.7 M NaCl (aq) can be found in the online version of the manuscript (Coccosphere_0.7 M_NaCl.avi). Note that in the timelapse videos, the extent of the "shrapnel" spread is entirely consistent with that expected for Brownian motion of the particles as opposed to any 'explosion' which might be falsely inferred from the sped-up video. Interestingly, in 0.7 M NaCl (aq), at equivalent ionic strength to that of seawater, the size of the coccosphere remains constant for approximately 1000 s before a rapid decrease in coccosphere size was seen. This is likely due to the ionic strength of the interior of the cell/cytoplasm being similar to that of seawater so no drive for osmotic change. Moreover, Walker *et al.*[28] reveals the presence of structured polysaccharide layers responsible for the rearrangement of the coccosphere which would otherwise not be present on individual detached coccoliths. In other words, *C. braaudii* coccosphere is not the sum of its constituent coccoliths but rather it is that plus a structured polysaccharide layer. Since the dissolution kinetics of living coccolithophores cannot be measured *via* the auto-dissolution approach, in either DI or high ionic strength solutions, we conclude that the dissolution of the coccolithophore is not the sum of its liths and inferring the PIC mass on living coccolithophores is beyond the limit of this technique.

It is noteworthy that, in our previous work, where electrochemically generated acid was used to infer the PIC mass of coccospheres; it requires only tens of seconds for the acid to dissolve the coccolithophore to completion.[18] Due to the much shorter timescale of the acid titration reaction, calcite 'shrapnel' were not observed to diffuse out from the coccosphere.

Conclusions

In this work, the PIC mass of individual *C. braarudii* coccoliths was obtained by imaging their auto-dissolution in DI water. Excellent agreement with literature reported values was seen. The non-esoteric set-up and simple experimental procedures allow coccolith mass measurements to be easily and routinely performed at a single-entity level by the widest oceanographer community. Interestingly, the auto-dissolution of detached coccoliths in DI water occurs at the mass-transport limit which is indistinguishable from that of an equivalently sized inorganic calcite particulate. This likely suggests that the coccolith compositions in terms of trace metal impurities and occluded organics are insignificant to affect the rate of its undersaturated driven dissolution. Nevertheless in seawater the roles of the diversity of dissolved matter may become significant; it is

thought for example that Mg^{2+} can inhibit calcite dissolution. Living coccolithophores, however, exhibit a different behaviour to a sum of its coccoliths likely due to the presence of structured polysaccharide layers responsible for the rearrangement of the coccosphere.

Author contributions

Conceptualization: TMC, MY, CBM, RGC, experiment: TMC (lead), SB (culture), methodology: TMC, MY, CBM, software: MY, CBM, formal analysis: TMC, visualization: MY, CBM, supervision: RGC, writing—original draft: TMC, MY, writing—review & editing: CBM, SB, RGC, REMR, HAB.

Conflicts of interest

There are no conflicts to declare.

Acknowledgements

References

1 F. J. Millero, *Chem. Rev.*, 2007, **107**, 308–341.

2 J. D. Milliman, *Global Biogeochem. Cycles*, 1993, **7**, 927–957.

3 K. M. Krumhardt, N. S. Lovenduski, M. C. Long, M. Levy, K. Lindsay, J. K. Moore and C. Nissen, *J. Membr. Biol.*, 2019, **11**, 1418–1437.

4 B. Rost and U. Riebesell, in *Coccolithophores*, Springer, 2004, pp. 99–125.

5 R. A. Armstrong, C. Lee, J. I. Hedges, S. Honjo and S. G. Wakeham, *Deep Sea Res., Part II*, 2001, **49**, 219–236.

6 C. Klaas and D. E. Archer, *Global Biogeochem. Cycles*, 2002, **16**, 63.

7 D. A. Hutchins, *Nature*, 2011, **476**, 41–42.

8 B. D'Amario, C. Pérez, M. Grelaud, P. Pitta, E. Krasakopoulou and P. Ziveri, *Sci. Rep.*, 2020, **10**, 1–14.

9 A. Oviedo, P. Ziveri and F. Gazeau, *Estuarine, Coastal Shelf Sci.*, 2017, **186**, 58–71.

10 G. Langer, M. Geisen, K. H. Baumann, J. Kläs, U. Riebesell, S. Thoms and J. R. Young, *Geochem., Geophys., Geosyst.*, 2006, 7.

11 P. R. Bown, J. A. Lees and J. R. Young, in *Coccolithophores*, Springer, 2004, pp. 481–508.

12 J. R. Young and P. Ziveri, *Deep Sea Res., Part II*, 2000, **47**, 1679–1700.

13 M. Yang, C. Batchelor-McAuley, S. Barton, R. E. Rickaby, H. A. Bouman and R. G. Compton, *Angew. Chem.*, 2021, **133**, 21167–21174.

14 M.-Á. Fuertes, J.-A. Flores and F. J. Sierro, *Mar. Micropaleontol.*, 2014, **113**, 44–55.

15 L. Beaufort, N. Barbarin and Y. Gally, *Nat. Protoc.*, 2014, **9**, 633–642.

16 L. Beaufort, *Micropaleontology*, 2005, **51**, 289–297.

17 J. Bollmann, *Biogeosciences*, 2014, **11**, 1899–1910.

18 M. Yang, C. Batchelor-McAuley, S. Barton, R. E. Rickaby, H. A. Bouman and R. G. Compton, *Environ. Sci.: Adv.*, 2022, **1**, 156–163.

19 T. Beuvier, I. Probert, L. Beaufort, B. Suchéras-Marx, Y. Chushkin, F. Zontone and A. Gibaud, *Nat. Commun.*, 2019, **10**, 1–8.

20 M. D. Keller, R. C. Selvin, W. Claus and R. R. Guillard, *J. Phycol.*, 1987, **23**, 633–638.

21 F. M. Morel, J. Rueter, D. M. Anderson and R. Guillard, *J. Phycol.*, 1979, **15**, 135–141.

22 OpenFrame: an open source approach to fluorescence microscopy, **https://www.imperial.ac.uk/photonics/research/biophotonics/instruments–software/fluorescence-microscopy/openframe/**.

23 X. Fan, C. Batchelor-McAuley, M. Yang and R. G. Compton, *ACS Meas. Sci. Au*, 2022, **2**(5), 422–429.

24 T. Hassenkam, A. Johnsson, K. Bechgaard and S. Stipp, *Proc. Natl. Acad. Sci. U. S. A.*, 2011, **108**, 8571–8576.

25 J. R. Young, S. A. Davis, P. R. Bown and S. Mann, *J. Struct. Biol.*, 1999, **126**, 195–215.

26 R. Wong, C. Batchelor-McAuley, M. Yang and R. G. Compton, *J. Electroanal. Chem.*, 2021, **903**, 115818.

27 C. S. Sikes and K. M. Wilbur, *Limnol. Oceanogr.*, 1982, **27**, 18–26.

28 C. E. Walker, A. R. Taylor, G. Langer, G. M. Durak, S. Heath, I. Probert, T. Tyrrell, C. Brownlee and G. L. Wheeler, *New Phytol.*, 2018, **220**, 147–162.

© 2023 The Author(s). Published by the Royal Society of Chemistry

Environ. Sci.: Adv., 2023, **2**, 645–651 | **651**